Theor. Comput. Fluid Dyn. (2011) 25:53–64
DOI 10.1007/s00162-010-0187-5

ORIGINAL ARTICLE

Gayathri Swaminathan · Kirti Chandra Sahu · A. Sameen · Rama Govindarajan

Global instabilities in diverging channel flows

Received: 11 May 2009 / Accepted: 3 December 2009 / Published online: 10 March 2010

Abstract A global stability study of a divergent channel flow reveals features not obtained hitherto by making either the parallel or the weakly non-parallel (WNP) flow assumption. A divergent channel flow is chosen for this study since it is the simplest spatially developing flow: the Reynolds number is constant downstream, and for a theoretical Jeffery–Hamel flow, the velocity profile obeys similarity. Even in this simple flow, the global modes are shown to be qualitatively different from the parallel or WNP. In particular, the disturbance modes are often not wave-like, and the local scale, estimated from a wavelet analysis, can be a function of both streamwise and normal coordinates. The streamwise variation of the scales is often very different from the expected linear variation. Given recent global stability studies on boundary layers, such spatially extended modes which are not wave-like are unexpected. A scaling argument for why the critical Reynolds number is so sensitive to divergence is offered.

Keywords Global stability analysis · Diverging channel

1 Introduction

Most shear flows are spatially developing, i.e. their velocity profile evolves as the flow proceeds downstream. Typically, as the Reynolds number increases, the laminar shear flow undergoes a linear instability, followed by an often complicated, and not completely understood, route to turbulence. Notable exceptions to this behaviour pattern are the flow through an infinite straight channel and that through an

Electronic supplementary material The online version of this article (doi:10.1007/s00162-010-0187-5) contains supplementary material, which is available to authorized users.

Communicated by T. Colonius

G. Swaminathan(✉), R. Govindarajan
Engineering Mechanics Unit, Jawaharlal Nehru Centre for Advanced Scientific Research, Bangalore, India
E-mail: gayathri@jncasr.ac.in

R. Govindarajan
E-mail: rama@jncasr.ac.in

K. C. Sahu
Department of Chemical Engineering, Indian Institute of Technology Hyderabad, Hyderabad, India
E-mail: ksahu@iith.ac.in

A. Sameen
Department of Aerospace Engineering, Indian Institute of Technology Madras, Chennai, India
E-mail: sameen@ae.iitm.ac.in

infinite straight pipe. The former is linearly stable up to a critical Reynolds number Re_{cr} of 5772 while the latter is linearly stable at any Reynolds number Re. Both these flows usually undergo a transition to turbulence at Reynolds numbers of 1500 or 2000. Recent decades have seen intense research activity to explain this apparent discrepancy and mechanisms relying on transient growth and/or non-linearity are offered.

However, in a flow differing in a small way from that through an infinite straight channel, such as with a small divergence of the channel walls, the mechanism of exponential growth could become important. The stability of laminar flow through this geometry known as Jeffery–Hamel flow [20] (JH hereafter) was first studied by Eagles [6]. Here a parallel flow approximation was made, i.e. the streamwise change in the channel width was neglected. Later work such as that of Sahu and Govindarajan [18] took this non-parallel effect into account but made some approximations which are valid at small angles of divergence, 2θ, as well as large Reynolds number. This general approach, which we refer to here as the weakly non-parallel (or WNP), has been adopted to study a wide variety of shear flows, e.g. Gaster [9], Bertolotti et al. [3] for boundary layers and Monkewitz et al. [14]. It assumes a disturbance of the form $\psi(x, y, t) = \phi(x, y) \exp i \left\{ \int \alpha(x) \mathrm{d}x - \omega t \right\}$, with the streamwise wavenumber α and downstream variation of the eigenfunction ϕ prescribed to be slowly varying functions of the streamwise coordinate x. By this it is implied that the disturbance has a locally wave-like form, i.e. the rapid portion of the downstream variation scales locally as α. The wall-normal coordinate is y, and ω is the complex frequency of the disturbance streamfunction ψ, whose imaginary part gives the temporal growth rate of the disturbance. Note that the parallel flow assumption would constitute taking α to be constant at every x and ϕ to be a function of y alone. At higher angles of divergence and/or low Reynolds numbers (of order 1), there is no reason to assume a priori that either of these quantities would vary slowly in x, or indeed that the disturbance would have a wave-like form in x.

Returning to the case of a channel, small amounts of wall divergence are well known to have a large effect on the stability (see e.g. [1,2,7,11,15,18,24]), and upon making the assumption of locally parallel flow, this dramatic dependence is captured to a great extent. McAlpine and Drazin [13] showed that while divergence drastically destabilizes the flow, convergence causes a huge stabilizaion. Dennis et al. [4] studied numerically the flow in a diverging channel enclosed between two arcs and found that the inlet and outlet conditions have a very strong influence on the non-linear development of the flow. Putkaradze and Vorobieff [17] studied the JH flows experimentally and demonstrated that a symmetric unidirectional outflow JH solution, if it exists, is always stable. Kerswell and Drazin [12] studied, using a theoretical model, the non-linear evolution of two-dimensional spatial waves in JH flows.

In the JH flow, the Reynolds number does not vary downstream, and the velocity profile is self-similar. One would therefore expect a disturbance of constant dimensionless wavelength, combined with a self-similar amplitude function $\phi(y)$, to satisfy the stability equations. Why then do we need to study this geometry as a global stability problem? We study it here to show how a global analysis can reveal fundamental characteristics of the instability which are not accessible to the parallel or WNP approaches. In fact none of the global instability modes resemble parallel or WNP modes. The point is that if the geometry, the pressure, or other relevant parameters were varying in a complicated fashion with x, one would not be surprised that global stability studies give results very different from the parallel. The fact that global modes can look qualitatively different in this, perhaps the simplest of non-parallel flows one could construct, is more interesting. This finding in JH flows may be contrasted with recent studies on boundary layers (e.g. [8]). There it is seen that global stability results do differ from WNP quantitatively, but a given mode is still described by a basic WKB structure, of a wave with a slowly changing wavelength streamwise. We highlight here only a few important aspects of the effect of two-dimensionality on the disturbance eigenfunction. In addition to the JH, we consider a more realistic geometry as shown in Fig. 2, where the mean flow is obtained numerically.

One reason for the global modes to display a much richer variety of modes than the parallel is that the disturbance eigenfunction obtained from solving the Orr-Sommerfeld equation can be multiplied by an arbitrary function of x and still satisfy the equation. In the case of global stability, the prefactor function of x is specified by the solution. We recently found this to have a large effect in the case of the wall jet [10]. Second, the solution there is often not a simple wave-like one, since wavelengths change from one y location to another and the solution at a particular spatial location cannot be described by a single wave. We wished to study only the effect of spatial development and not of streamwise changes in Reynolds number. This is one main motivation for this study.

2 Mean flow

We consider flow through two geometries: the JH flow (Fig. 1) and a more realistic shape, similar to those studied by Nakayama (see [5]) and Tutty [22], with a finite diverging section (Fig. 2) where Neumann boundary conditions are applicable for the mean flow at the inlet and exit.

The steady laminar two-dimensional flow of incompressible fluid within an infinite wedge driven by a line source/sink situated at the intersection of the rigid planes that form the wedge (Fig. 1) was first described by Jeffery (1915) and Hamel (1916) (see, e.g. [20]), by the similarity equation

$$U''' + 2SUU' + 4\theta^2 U' = 0, \tag{1}$$

$U(+1) = U(-1) = 0$; $U(0) = 1$. Here U is the mean velocity in the similarity coordinate $\eta = (y/H(x))$, θ is the semi-divergence angle as shown in Fig. 1, H is the channel half-width, the primes stand for differentiation with respect to η, $S \equiv \theta Re$, x is the streamwise co-ordinate and y is the wall-normal co-ordinate. As mentioned before, the Reynolds number (defined as $Re \equiv U_c(x)H(x)/\nu$, where the subscript 'c' stands for the channel centreline and ν for kinematic viscosity) is constant downstream, in contrast to most developing shear flows. The velocity profile is obtained using the fourth-order Runge-Kutta method with 10,000 grid points. The flow displays a separated region for S greater than 10.3. The domain over which global stability computations are performed is shown in Fig. 1. The starting point in the x direction of this domain follows the relation $x_{\text{start}}/H_1 = 1/\tan(\theta)$. The domain extends up to $x_{\text{end}} = x_{\text{start}} + L$, where L is set equal to 50π, unless otherwise specified. All quantities are non-dimensionalized by the centreline velocity at the inlet U_i, and the half-channel width H_i at the inlet.

The mean velocity profile for the channel with the finite divergent section (referred to hereafter as SDS for straight-divergent-straight, Fig. 2) is obtained by a numerical solution of the streamfunction–vorticity formulation of the two-dimensional Navier–Stokes equation. At each Re and θ, it is ensured that the final straight section is long enough for the flow to attain a parabolic profile well before the exit. The length of this exit straight section increases approximately linearly with increasing Reynolds number. Therefore the mean velocity profile computations can become very time consuming. To speed up the computations, a multi-grid technique is used, and a fast parallel solver incorporated, details of which are available in [23]. In the present computations, the divergence starts at $x = 9.37$ and ends at $x = 91$, as shown in Fig. 2.

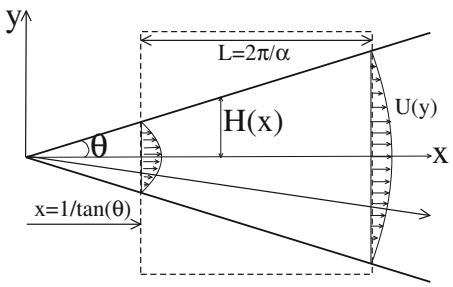

Fig. 1 Schematic of Jeffery–Hamel flow originating from a point source at the origin. θ is the semi-divergence angle in degree and x is the streamwise co-ordinate. Note that the axes are non-orthogonal. For global stability computations, the inlet of the two-dimensional domain is fixed at a distance of $1/\tan(\theta)$, as the length scale of the problem is the inlet half-width. The two-dimensional domain over which the global stability computations are made is shown by the *rectangular box*

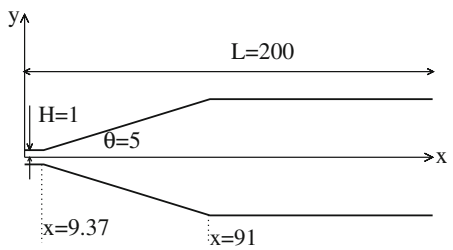

Fig. 2 Schematic of the channel with the finite divergent section, referred to here as SDS. The exit straight region is kept sufficiently long to achieve parabolic velocity profile at the exit

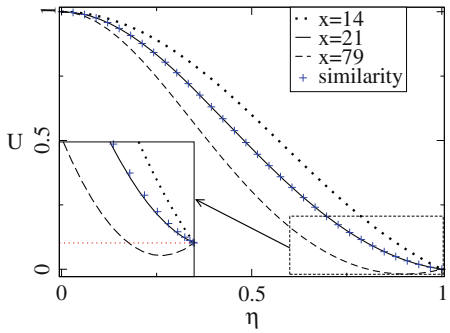

Fig. 3 Comparison of the mean velocity profiles of JH flow (shown in Fig. 1) with those of SDS flow (Fig. 2) at a few streamwise locations. The symbols are for a similarity solution with $S = 8.72(Re = 100, \theta = 5°)$. The *lines* are for the SDS channel at different x locations. It can be seen that the JH profile matches with the numerical profile for the SDS channel at $x = 21$

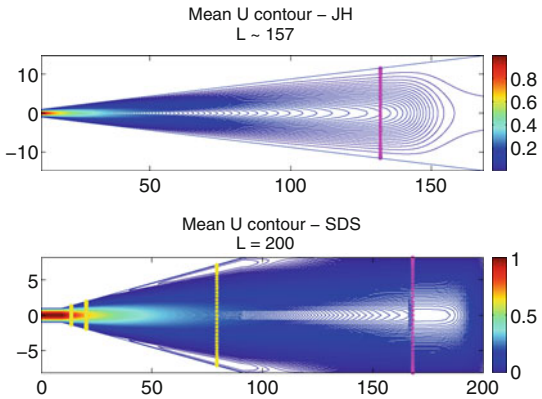

Fig. 4 Comparison of mean streamwise velocity contours of JH and SDS flows, for the case shown in Fig. 3. Note the region of weak separation in the SDS case. The vertical line (in *magenta*) towards the exit of the domain indicates the location at which the sponging starts. The sponging smoothly reduces the local Reynolds number as a hyperbolic tangent function. The three vertical lines (in *yellow*) in the diverging region of the SDS channel indicate the three streamwise locations discussed in Fig. 3 (color figure online)

For a half-angle of divergence of five degrees, and a Reynolds number of 100, the profiles obtained for the similarity Eq. 1 and the SDS channel are presented in Fig. 3. A domain length of $L = 200$ is found to be sufficient to get a parabolic flow at the exit. Plotted here is the streamwise velocity U versus the non-dimensional co-ordinate η. The lines shown in the figure are obtained for SDS at three different x locations and the symbols are the solutions of Eq. 1 for $S = Re\theta = 8.72$. We note that the JH profile is not separated at this S value, whereas the SDS profile is separated downstream due to centreline acceleration caused by the divergent section being finite. Contours of the mean streamwise velocity distribution are shown in Fig. 4. A region of weak separated flow extending over most of the divergent portion can be discerned in the SDS. To avoid any spurious reflections of the disturbance modes from the exit, a sponging is applied over a region just upstream of the exit, details of which are given in Sect. 3. The contours in the figure are obtained by applying a sponging over 30% of the domain, the vertical line (in magenta) towards the exit of the domain indicates its starting location. The three vertical lines (in yellow) in the SDS domain indicate the three streamwise locations mentioned in Fig. 3.

3 Formulation and numerical method

Adding a disturbance streamfunction of the global form, $\psi = \phi(x, y)e^{-i\omega t}$ to the mean streamfunction, substituting in the Navier–Stokes equations for incompressible flow and linearizing, we get the two-dimensional stability equation for the disturbance streamfunction as,

$$\left[U\left[\frac{\partial}{\partial x}\left(\frac{\partial^2}{\partial x^2}+\frac{\partial^2}{\partial y^2}\right)\right]+V\left[\frac{\partial}{\partial y}\left(\frac{\partial^2}{\partial x^2}+\frac{\partial^2}{\partial y^2}\right)\right]+\left[\frac{\partial^2 V}{\partial x\partial y}-\frac{\partial^2 U}{\partial y^2}\right]\frac{\partial}{\partial x}+\left[\frac{\partial^2 U}{\partial x\partial y}-\frac{\partial^2 V}{\partial x^2}\right]\frac{\partial}{\partial y}\right.$$
$$\left.-\frac{1}{Re}\left(\frac{\partial^2}{\partial x^2}+\frac{\partial^2}{\partial y^2}\right)^2\right]\phi=\left[i\omega(\frac{\partial^2}{\partial x^2}+\frac{\partial^2}{\partial y^2})\right]\phi$$

where ϕ is the two-dimensional disturbance amplitude and ω is the eigenvalue.

This equation is discretized with n and m points in the x and y directions, respectively. We have checked that $m = 41$ points are sufficient, and $n = 121$ and $n = 221$ are in good agreement for the results presented within the parameter ranges considered. We have used Chebyshev spectral collocation in both directions. This clusters the grid points close to the walls in the wall-normal direction (which is desirable), and close to the inlet and exit of the domain (which is not desirable). Hence the grids are stretched in x to give a more or less uniform distribution of points in the streamwise direction. The stretching function used is

$$x_j = \frac{a}{\sinh(bx_0)}[\sinh((x_c - x_0)b) + \sinh(bx_0)], \tag{2}$$

$$x_0 = \frac{0.5}{b}\log\left[\frac{(1+(e^b-1)a)}{(1+(e^{-b}-1)a)}\right]. \tag{3}$$

Here, x_c is the collocation point, a is the location around which clustering is required and b is the degree of clustering. After several trials for better accuracy, their values are fixed to be $a = 0.5, b = 3.0$. The discretization results in a large non-symmetric, real, dense matrix eigenvalue problem of size $nm \times nm$, solved using the library LAPACK which adopts the QZ algorithm.

3.1 Boundary conditions

No-slip and no-penetration boundary conditions on both the walls are prescribed. The streamwise boundary conditions to be applied are not obvious, and moreover, can have a strong influence on the results. We aim to minimize this influence. This is one important reason for including study on an SDS channel, in which the region of disturbance growth may be expected to be localized around the divergent portion, and the flow far upstream and downstream to be stable at the Reynolds numbers we consider. In an SDS channel therefore, especially one with a long straight section at the exit, we have at least two options for streamwise boundary conditions, namely Neumann and extrapolated boundary conditions (EBCs), at both the inlet and the exit. In several studies of this type, the Robin boundary conditions are used [8], where wave-like behaviour is prescribed, if necessary with different wavelengths fixed at the inlet and the exit. We note however that since the global mode is not necessarily wave-like, the Robin boundary conditions would be inappropriate (except for comparison with local stability approaches).

Following [21] we settle for EBC, as we see it as being the least prejudicial, both for JH and SDS. All disturbance quantities at the boundary are prescribed to be linear extrapolations of their values in the interior of the domain. For example, the wall-normal velocity ϕ_x at the inlet, say (1), is written as a linear function of the values at the next two grid locations (2,3) as,

$$\phi_{x1}[x_3 - x_2] - \phi_{x2}[x_3 - x_1] + \phi_{x3}[x_2 - x_1] = 0 \tag{4}$$

Similarly, the value at the exit can be written as a linearly extrapolated function of the values prior to the exit. It is found that if a sufficiently long domain is considered, the precise form of the boundary conditions does not affect the results. Unless otherwise mentioned, the above-mentioned EBCs are used for all the results presented.

Our computations on other geometries like wall jets with the EBCs had shown reflections from the boundaries. To avoid such spurious reflections, if any, a sponge is applied at the exit of the domain. This is achieved by artificially decreasing the local Reynolds number in the exit region, using a smooth function, say a hyperbolic tangent. Since this was done by reducing the mean velocity, this region does not conserve mass flux. The sponging strength is defined as the ratio of the decrease in the Reynolds number between the flow and the exit, to the Reynolds number of the flow. Sponging strengths of between 50 and 90% have been used. The sponged length is the fraction of the domain over which the sponging is applied. For the SDS case, it is ensured that the sponging is applied only in a portion of the exit straight region, with sponged lengths ranging from 20 to 40%. Within this range of strengths and lengths, it is seen that the results remain insensitive as discussed below.

4 Results and discussion

For the purpose of preliminary comparisons of the global stability approach with the parallel or WNP stability, and also to contrast with more realistic computations made later, we begin with a JH flow on a domain whose streamwise length is fixed as the wavelength of the least stable mode in the parallel or WNP stability results. Further, a wave-like nature of the disturbance is forced at the inlet and exit of the channel by using Robin boundary conditions. We use $(D_{xx}\phi)_{1,n} = -\alpha_{1,n}^2\phi_{1,n}$ for all y locations, where D_{xx} is the discretized form of $\partial^2/\partial x^2$, and similar conditions on the fourth derivative in the streamfunction. The subscripts 1 and n correspond to the inlet and exit, respectively. Even-order derivatives are chosen so as to remain in the real plane and thus speed up computations. The choice of α at each boundary is not obvious, and we have made this choice in two ways, as described below. In the parallel and WNP approaches, the definition of critical Reynolds number is a local one. Since the Reynolds number is constant everywhere in this flow, the dimensionless wavenumber and frequency (based on local length and velocity scales) of the least stable mode obtained by the parallel or WNP are constant too. This means that the *dimensional* wavenumber and frequency depend on the streamwise location. We may match the wavenumber α_1 at the entry with the parallel or WNP α. At the exit, we may either match the dimensional wavenumber, or prescribe a wavenumber corresponding to the same dimensional frequency as at the inlet, but cannot match both. The first is done by matching α_1 with the parallel result, and setting α_n/α_1 equal to the ratio of the exit and entry half-widths. Since the streamwise extent of this domain is limited, grid insensitive results are obtained in this case with only $n = 51$ and $m = 41$. We begin by validating the global approach by setting $\theta = 10^{-12}$ degree and $L = 2\pi/1.02056$, and obtain the standard value of $Re_{\rm cr} = 5772$ [16] on a straight channel. The eigen functions also match with very good accuracy. At higher angles too, with the domain size matched each time to the wavelength of the least stable parallel mode, the $Re_{\rm cr}$ of the global stability computations compare reasonably with parallel results, as seen in the circles (in red) of Fig. 5.

The other option is exercised by setting α_1 to the critical WNP value. To find α_n at the exit corresponding to the same *dimensional* frequency as at the inlet, we iterate the WNP computation in α until we converge on a least stable α whose frequency is equal to $\omega_1(x_n/x_1)^2$, where ω_1 is the critical WNP frequency corresponding to α_1. This fixation of the exit wavenumber is seen to predict a smaller $Re_{\rm cr}$ at larger θ, as seen by the squares (in blue) of Fig. 5.

The restriction of the domain size and the prescription of a wave-like nature of the perturbations at the entry and exit, that too of a fixed wavelength, mean that the critical Reynolds numbers predicted by the global computations are not likely to be realistic, so the main purpose of this exercise is to validate the global stability approach as best we can. The later results in this paper use a much larger streamwise domain, with EBCs, to correspond better with reality. Before we discuss these, we briefly investigate why the $Re_{\rm cr}$ is so sensitive to divergence, especially close to zero divergence. To explain this, we expand the mean flow at small divergence as a perturbation of the Poiseuille solution. At $S \ll 1$, we may write the solution to Eq. 1 as

$$U = 1 - y^2 + S(-y^6/30 + y^4/6 + 2/15y^2). \tag{5}$$

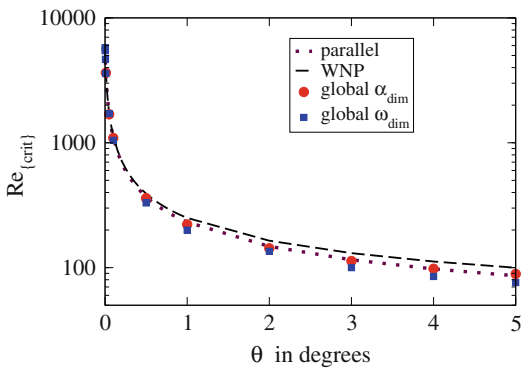

Fig. 5 Variation of critical Reynolds number with divergence angle in JH flow. The circles (in *red*) stand for the global analysis results with Robin boundary conditions holding the dimensional wavenumber the same at both inlet and exit. The domain size and inlet wavenumber are matched with parallel results at each angle. The squares (in *blue*) are obtained by matching inlet conditions and domain size with WNP, and holding the exit wavenumber at the WNP value corresponding to the same dimensional frequency as the inlet (color figure online)

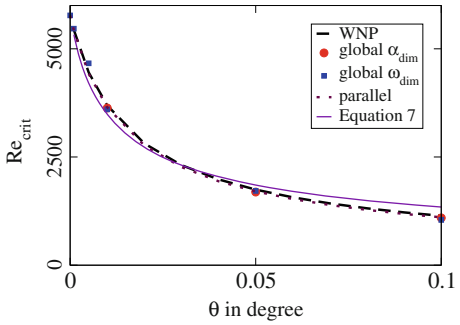

Fig. 6 Sensitivity of $Re_{\rm cr}$ to the divergence angle θ at very small θ. Equation 7 obtained from perturbing about the Poiseuille solution is reasonable at predicting the rapid decrease of $Re_{\rm cr}$ with increase in θ

At the critical Reynolds number, the non-parallel operator for a very small angle may be written as

$$\mathrm{Ra_P}\phi + 1/Re_{\rm cr}(\phi^{\rm iv} + \text{higher order terms}) + i\alpha\Delta U''\phi. \tag{6}$$

$\mathrm{Ra_P}$ stands for the Rayleigh operator for Poiseuille flow. Neglecting the change with θ in the eigenvalue and the eigenfunction ϕ, we get an approximate equation for the $Re_{\rm cr}$ as a function of the divergence angle θ, as

$$\frac{1}{Re_{\rm cr}^2} - \frac{1}{5772^2} = 3 \times 10^{-4}\theta. \tag{7}$$

The constant on the right-hand side is obtained from the Orr-Sommerfeld solution. Figure 6 shows that the above equation, which is entirely obtained from the Poiseuille flow solution, does reasonably well in explaining why the critical Reynolds number drops steeply at low divergence angles.

We now study both the infinitely diverging (self-similar) JH flows and the SDS flows using the EBCs, for different combinations of Reynolds numbers, $Re = 50, 100, 200$ and divergence angles, $\theta = 0.001°, 2°, 5°$. Results presented henceforth use a grid of 221×41. The domain length for JH is $L \sim 157$ and for SDS is 100, 200 and 400 for Reynolds numbers 50, 100 and 200, respectively. The sponged lengths and sponging strengths are mentioned where appropriate. Comparisons of the spectra obtained for JH and SDS flows are shown in Figs. 7 and 8, respectively. It is immediately clear that the spectra have distinct branches, and we will see that modes in corresponding branches have similar structure. Increase in θ as seen in Fig. 7 pushes the spectrum towards instability as expected. The modes in the distinct branches remain very insensitive to different sponge strengths, sponging lengths and grid size. However, the spectra contain a few isolated eigenvalues close to the axes, which move significantly with changes in these parameters. Moreover the corresponding eigenfunctions were found to be spurious by visual examination. We do not discuss these spurious modes further, and restrict our attention to modes in the distinct branches. Increase in the Reynolds number (Fig. 8) increases the frequency of the most unstable modes, i.e. the different branches are stretched in the x-axis. The level of instability at this θ is not too sensitive to the Reynolds number within this range.

We now focus our attention on the JH flow at $Re = 100$ and $\theta = 5$ degree. According to WNP, the $Re_{\rm cr}$ for this flow is 99.88, and a near-neutral situation is a good candidate for study. Our motivation however is not to merely obtain a number for the critical Reynolds number, but to understand the characteristic features of the instability resulting from the spatial development of the flow, so the choice is not crucial. The spectrum with a sponged length of 20% and a sponging strength of 90% is shown in Fig. 9. The two near-neutral discrete modes seen are spurious, as discussed above, and they are not obtained with other grid resolutions. As mentioned before, the spectrum contains several distinct branches, and four of these, marked as B1 to B4, are chosen for further consideration. The modes in each of these branches have a characteristic structure unique to that branch. One typical mode from each branch is shown in Figs. 10 and 11. We emphasize that the eigenvalues and eigenfunctions of these branches remain very insensitive to different lengths of the domain, sponge strength and extent of sponged region. Moreover they are the same whether Neumann or EBC boundary conditions are used. The nature of these modes reveals that the employment of Robin boundary conditions, resulting in forcing a wave-like solution, as we did earlier for comparison with parallel studies, and as often adopted in studies of spatially developing flows, is inappropriate. It is found that the production layer of the modes in B1 and B2 (not shown) is localized in streamwise extent. The modes in B3 extend all over the domain and are dominant close to the centreline, while those of B4 are closer to the wall.

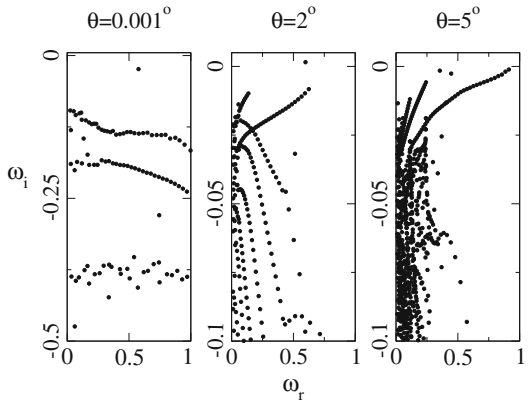

Fig. 7 Spectra for JH at $Re = 100$ for different θ. There is an overall destabilization with increase in divergence. It is seen that with increase in θ, branches which tended to point downwards at high frequency begin to point upwards, so at higher divergence, it is the higher frequency modes which are less stable

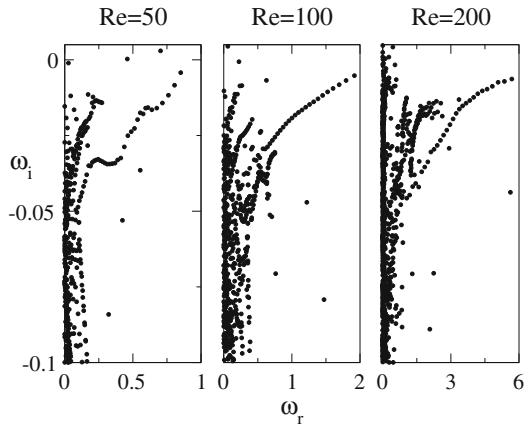

Fig. 8 Spectra for SDS at $\theta = 5$ for different Reynolds numbers. Again some distinct branches can be discerned. The frequency of corresponding branches increases with Reynolds number

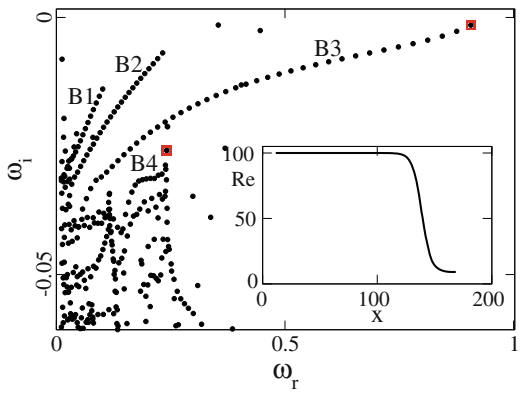

Fig. 9 Spectrum for JH flow at $\theta = 5°$, $Re = 100$, $L = 157$, grid size 221×41, with 90% sponge strength, applied over 20% of the domain. The modes in branches B1 to B4 each have characteristic features, as will be seen. The Reynolds number is shown in the inset as a function of the streamwise distance, indicating the sponging applied

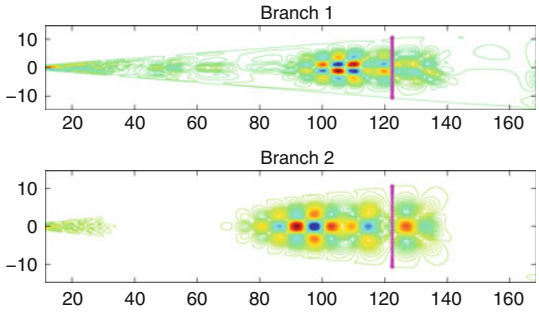

Fig. 10 Contours of streamwise velocity of typical modes in branches B1 and B2 of Fig. 9. In this and subsequent figures, the vertical line (in *magenta*) towards the exit indicates the location at which the sponging begins (color figure online)

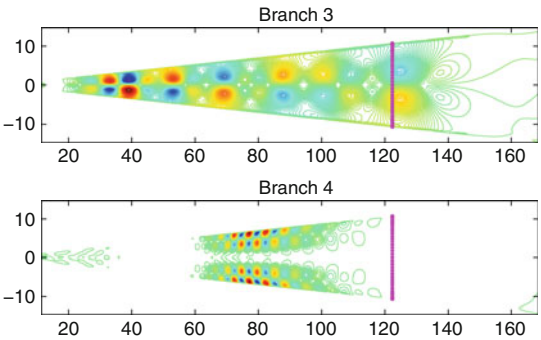

Fig. 11 Contours of streamwise velocity of typical modes in branches B3 and B4 of Fig. 9. The modes in branch B3 often display multiple positive peaks in succession followed by an equivalent number of negative peaks, emphasizing that they are not wave-like

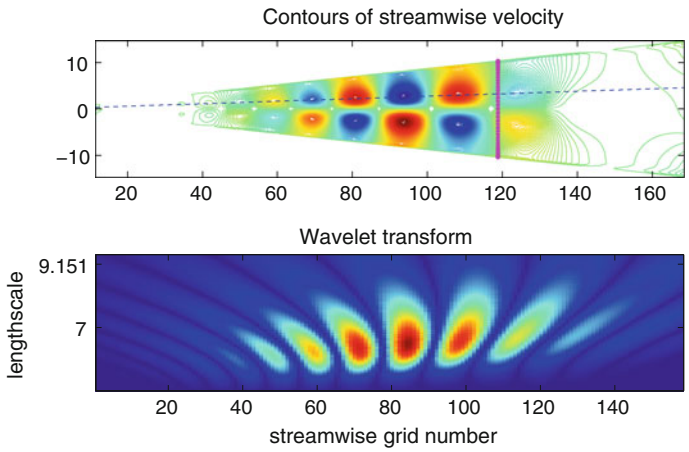

Fig. 12 *Top*: Streamwise velocity contour of the mode indicated by a (*red*) square in branch B3 in Fig. 9, with $\omega = (0.90640, -0.0014952)$. *Bottom*: Wavelet transform of the mode shown on top at the wall-normal location indicated by the horizontal (*blue*) dashed line. Please note, figures discussing wavelet transform are not to scale (color figure online)

Since it is not straightforward to estimate by visual examination the length scales of the disturbance modes at various locations in the domain, a wavelet transform is carried out to get quantitative information. At a given wall-normal location, an eigenfunction of a perturbation quantity such as the streamwise velocity perturbation is a function of x. The amplitude of the wavelet transform indicates the contribution to each length scale of a mode at a given streamwise location, so that the brightest spot at a given streamwise station indicates the dominant length scale at that location. Morl wavelet has been used in the results presented here, but the answers are not very sensitive to the specific choice. The streamwise velocity distribution of two modes indicated by the squares (in red) in Fig. 9 is shown together with their wavelet transforms, with the one from B3 in Fig. 12 and the one from B4 in Fig. 13.

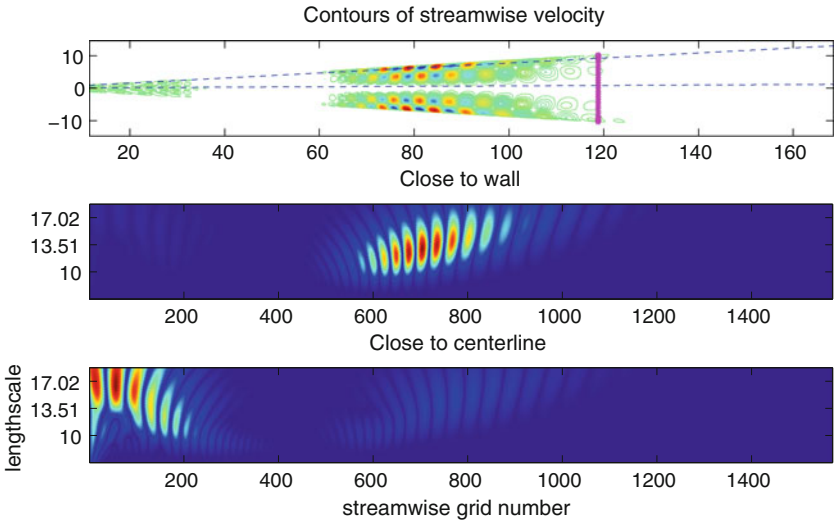

Fig. 13 *Top*: Streamwise velocity contour of the mode indicated by a (*red*) square in branch B4 in Fig. 9, with $\omega = (0.241297, -0.0258524)$. *Center and bottom*: Wavelet transforms of the mode shown on top at two wall-normal locations indicated by the two horizontal (*blue*) dashed lines, one close to wall and one close to the centreline (color figure online)

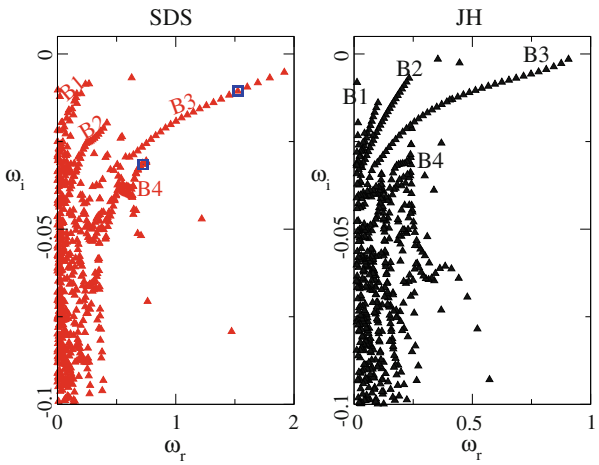

Fig. 14 Spectra of JH and SDS flows at $Re = 100$ and $\theta = 5$. Modes in the corresponding branches marked as B1, B2, etc., have similar mode structure, but with higher frequency in the SDS case

The B4 mode shown in Fig. 13 has an appearance very similar to its fellow mode from the same branch seen in Fig. 11. Its wavelet transform shows that the structure of the mode is a strong function of both x and y. Close to the wall, there is a region where the perturbation may seem locally wave-like, with a linear increase in wave-length as would be anticipated by a WNP type study. However, this expectation is belied by the wavelet transform of the perturbation closer to the centreline. The action at this y is closer to the inlet, with no discernible wave-like pattern. It is also evident that, in addition to one dominant length scale, there is energy contribution at several other sub-dominant length scales at a single streamwise station. A wavelet study has made it possible to arrive at this finding. Incidentally, such large variation of the dominant length scale within a given mode with x and y has also been seen in wall jets [10].

The B3 mode in Fig. 12 looks practically wave-like and appears different from the sample that was seen in Fig. 11. This mode is the least stable on that branch, and as we move to the left on B3 we see a gradual change in behaviour towards the sample shown earlier. Also, the resemblance of this least stable mode to a WNP wave is merely superficial. First, unlike a WNP mode, the dominant length scale does not vary too much with streamwise location. This shows that global restructuring is taking place. Second, while all the modes in the other branches evolve in time by moving downstream, the modes in branch B3 move upstream in time. This upstream propagation persists without change even with the application of extreme levels of sponging

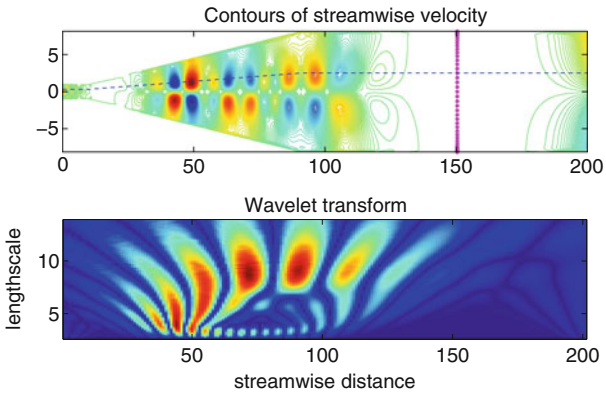

Fig. 15 *Top*: Streamwise velocity contour of the mode indicated by a (*blue*) square in branch B3 of Fig. 14, with $\omega = (1.524556, -1.059208E-002)$. *Bottom*: Wavelet transform of the mode shown on top at the wall-normal location indicated by the horizontal (*blue*) dashed line (color figure online)

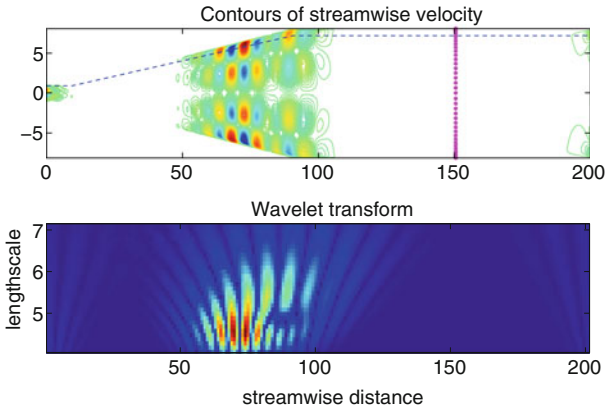

Fig. 16 *Top*: Streamwise velocity contour of the mode indicated by a (*blue*) square in branch B4 of Fig. 14, with $\omega = (0.7217860, -3.150661E-002)$. *Bottom*: Wavelet transform of the mode shown on top at the wall-normal location indicated by the horizontal (*blue*) dashed line (color figure online)

(not shown). Moreover upstream movement in the B3 branch is seen at all Reynolds numbers considered at this divergence, and also for two degrees. They are however absent in the case of 0.001 and 10^{-12} degrees of divergence. While we do not expect a strict adherence of the modes in this flow to standard behaviour such as the obedience of Howard's semi-circle theorem, the physical relevance/importance of this branch of modes is unclear at this time, and is being investigated.

We now examine a global spectrum at the same Reynolds number and divergence angle in the SDS channel. The sponging strength is 80% and sponging is applied over 25% of the domain length. A comparison of the spectra of JH and SDS is shown in Fig. 14. The dominant instability is decided by the divergent portion. The length of the divergent portion in JH flow without sponging is about 125, while in SDS it is about 80, which is comparable. We know from parallel and WNP that the frequency depends strongly on divergence. The straight portion therefore will have a significant effect on the overall frequency of the modes. We may thus expect, and find, a spectrum whose frequencies differ significantly. However, the mode structure remains qualitatively the same. Also, it is seen that the SDS channel is more stabilized than the JH in the sense that the growth rates of corresponding branches/modes have come down in the SDS case. This may be attributed to the presence of a straight region at the exit. Even though the SDS flow contains a region of separation, we see that the overall de-stabilizing effect of the weak separation region is smaller than the stabilizing effect of the straight region.

Two modes corresponding to branches B3 and B4 and indicated by (blue) squares in Fig. 14 are plotted in Figs. 15 and 16. We see a striking resemblance with the JH modes. Again the SDS mode in Fig. 15 has multiple positive and negative amplitudes in succession, exhibiting a non-wave-like behaviour. The wavelet transform of the above two modes also show similar trends as in the JH case. However, note that in both B3 and B4 there is significant contribution from the small scales over a range of x in addition to the large scales.

5 Conclusions

Global stability analysis is conducted on the simplest spatially developing flow one can construct, namely a channel of constant divergence, to show that the disturbances are not wave-like in the streamwise direction even in this similarity flow of constant Reynolds number. Given earlier global stability studies on boundary layers, where there is no such qualitative difference between global modes and parallel or WNP modes, this result is unexpected. In fact, although many global studies exist on spatially developing flows, spatially extended but non-wave-like modes are not commonly seen. Not only therefore is a WKB-type approach inadequate to study such flows, the application of Robin boundary conditions, as is common in studies of this type, is inappropriate.

More remarkable than the variation in streamwise length scale, which is not as expected from classical approaches, is the fact that energy-carrying scales are a function of the wall-normal direction, and that there can be several relevant length scales at one streamwise location. We hope that this work motivates studies aimed at a theoretical understanding of such behaviour, and also experiments which check these predictions. The modes obtained here would lend themselves to interesting transient growth characteristics in space and time. This aspect is being investigated, and could be especially interesting in the light of the WNP results of [19], where it was found that transient growth is not at all sensitive to wall divergence.

Acknowledgements We gratefully acknowledge the Defence R& D Organization, India, for financial support.

References

1. Allmen, M.J., Eagles, P.M.: Stability of divergent flow: a numerical approach. Proc. R. Soc. Lond. A **392**, 359–372 (1984)
2. Banks, W.H.H., Drazin, P.G., Zaturska, M.B.: On perturbations of Jeffrey-Hamel flow. J. Fluid Mech. **186**, 159 (1988)
3. Bertolotti, F., Herbert, T., Spalart, P.: Linear and nonlinear stability of the Blasius boundary layer. J. Fluid Mech. **242**, 441–474 (1992)
4. Dennis, S.C.R., Banks, W.H.H., Drazin, P.G., Zaturska, M.B.: Flow along a diverging channel. J. Fluid Mech. **336**, 183–202 (1997)
5. Drazin, P.G.: Flow through a diverging channel: instability and bifurcation. Fluid Dyn. Res. **24**, 321–327 (1999)
6. Eagles, P.M.: The stability of a family of Jeffery-Hamel solutions for divergent channel flow. J. Fluid Mech. **24**, 191–207 (1966)
7. Eagles, P.M., Weissman, M.A.: On the stability of slowly varying flow: the divergent channel. J. Fluid Mech. **69**, 241–262 (1975)
8. Ehrenstein, U., Gallaire, F.: On two-dimensional temporal modes in spatially evolving open flows: the flat-plate boundary layer. J. Fluid Mech. **536**, 209–218 (2005)
9. Gaster, M.: On the effects of boundary layer growth on flow stability. J. Fluid Mech. **66**, 465–480 (1974)
10. Gayathri, S., Sameen, A., Govindarajan, R.: Global instabilities in wall jets. In: Proceedings of the Seventh IUTAM Symposium on Laminar Turbulent Transition, Stockholm
11. Hamadiche, M., Scott, J., Jeandel, D.: Temporal stability of Jeffery-Hamel flow. J. Fluid Mech. **268**, 71–88 (1994)
12. Kerswell, R.R., Tutty, O.R., Drazin, P.G.: Steady nonlinear waves in diverging channel flow. J. Fluid Mech. **501**, 231–250 (2004)
13. McAlpine, A., Drazin, P.G.: On the spatio-temporal development of small perturbations of Jeffery-Hamel flows. Fluid Dyn. Res. **22**, 123–138 (1998)
14. Monkewitz, P.A., Huerre, P., Chomaz, J.M.: Global linear stability analysis of weakly non-parallel shear flows. J. Fluid Mech. **251**, 1–20 (1993)
15. Nakaya, C., Hasegawa, E.: Stability of steady flow in a diverging channel. Phys. Fluids **13**(12):2904–2906 (1970)
16. Orszag, S.A.: Accurate solution of the Orr-Sommerfeld stability equation. J. Fluid Mech. **50**, 689–703 (1971)
17. Putkaradze, V., Vorobieff, P.: Instabilities, bifurcations, and multiple solutions in expanding channel flows. Phys. Rev. Lett. **97**, 144502 (2006)
18. Sahu, K.C., Govindarajan, R.: Stability of ow through a slowly diverging pipe. J. Fluid Mech. **531**, 325–334 (2005)
19. Sahu, K.C., Sameen, A., Govindarajan, R.: The relative roles of divergence and velocity slip in the stability of plane channel flow. Eur. Phys. J. Appl. Phys. **44**, 101–107 (2008)
20. Schlichting, H.: Boundary Layer Theory, 8th edn. Springer, New York (2000)
21. Theofilis, V.: Advances in global instability analysis of nonparallel and three dimensional flows. Prog. Aerospace Sci. **39**, 249–315 (2003)
22. Tutty, O.R.: Nonlinear development of flow in channels with non-parallel walls. J. Fluid Mech. **326**, 265–284 (1996)
23. Venkatesh, T.N., Sarasamma, V.R., Rajalakshmy, S., Sahu, K.C., Govindarajan, R.: Super-linear speedup of a parallel multigrid navier-stokes solver on flosolver. Curr. Sci. **88**(4), 589–593 (2006)
24. Uribe, F.J., Bravo, A., Peralta-Fabi, R.: On the stability of Jeffery-Hamel flow. Phys. Fluids **9**(9), 2798–2800 (1997)